Crack branching and deflection in AISI 4340 steel under cyclic torsional loading

Z.K. Xu, B. Wang, P. Zhang*, X.Z. Gu and Z.F. Zhang*

Shi-changxu Innovation Center for Advanced Materials, Institute of Metal Research, Chinese Academy of Sciences, Shenyang 110016, China

Abstract

The high-cycle torsional fatigue crack propagation behaviors of the martensitic AISI 4340 steel were investigated in this work. Quantitative analyses of fracture processes were conducted to establish the branching mechanisms in the early crack propagation stage and the deflection in the later crack propagation stage. It was found that when the mode I stress intensity factor was greater than the threshold value $K_{\mathrm{I,th}}$, the initiated crack would branch off to four cracks in mode I. Furthermore, there is a competitive relationship among different pairs of branches. Firstly, the backward pair of branches encountered more boundary barriers. Secondly, their driving force was reduced by the stress redistribution caused by the leading pair of branches. In addition, due to the restriction of the grips, the crack would gradually turn into mode II from mode I. When $K_{\mathrm{II}}/K_{\mathrm{I}} > 1.5$, the cracks growth type became complete mode II.

Keywords: AISI 4340 steel; Torsional fatigue; Crack branch; Fracture mechanisms; Lath martensite.

* Corresponding authors.
E-mail addresses: pengzhang@imr.ac.cn (P. Zhang), zhfzhang@imr.ac.cn (Z. F. Zhang).

1. Introduction

There are many shaft components in vehicles subjected to cyclic torsional loading. The fatigue failure of those components often leads to the increasing need for the study of fatigue crack initiation and propagation behaviors under cyclic torsional loading [1-4]. Unlike the tension-compression loading, the fatigue crack under torsional loading has great changes during the crack propagation process [5]. Specifically, under tension-compression loading, the crack growth process could be divided into two stages. 1) The early mode II propagation, which is mainly affected by the microstructure, is called as stage I propagation. 2) The subsequent mode I propagation, in which the fatigue crack usually would not branch off or be deflected, is called as stage II propagation. In the same way, the fatigue crack under torsional loading would also undergo the stage I propagation affected by the microstructure and then turn into mode I propagation. However, under torsional loading, there are two problems different from the tension-compression loading in the fatigue crack growth behaviors. 1) During the stage I propagation, the crack would branch off into multiple mode I cracks. 2) Amid the stage II propagation, the crack would be deflected from mode I into mode II.

For the branching behavior in the early propagation, there are different performances in different materials [6-15]. The fatigue cracks in steels reported by Murakami et al [15], Zhang et al. [12], Schönbauer et al. [6, 8], Karr et al. [16], Akiniwa et al. [11] and Marquis et al. [17] would branch off in the early propagation. In addition, Zhang et al. [12] reported that the crack length in the branching point was related to the

loading stress. Schönbauer et al. [6, 8] found that the branching occurred after the initiated crack in δ ferrite encountered the tempered martensite matrix. As for the aluminum alloys, Serrano-Munoz et al. [18] found that the fatigue cracks in them would not branch off. For copper, the experimental results of Xu et al. [19], Li et al. [20-22] and Hofmann et al. [23] showed that there was no branching in the early propagation stage. After the review of the above researches, it is clear that the fatigue crack branching in the early propagation stage is common in steels, which might be related to the complex microstructure leading to local anisotropy. However, the fatigue crack branching behavior is seldom investigated. Revealing the bifurcation mechanism will help to improve the understanding of the whole process of fatigue damage, and thus propose methods to improve the fatigue performance.

For the deflection from mode I to mode II in stage II propagation, it could be found in several researches including solid cylinder specimens [1] and thin-walled tubular specimens [5, 9, 24]. Singh el al. [5] described the deflection behavior of the fatigue crack and defined the related quantities. However, the experiment was carried out under bending-torsional loading [5], and the bending stress would affect the deflection behavior. As for the fatigue crack deflection under pure cyclic torsional loading, the corresponding mechanisms are still unclear up to now.

This study presents both macroscale and microscale experimental investigation on the fatigue damage behavior in solid cylinder specimens of AISI 4340 steel subjected to pure cyclic torsional loading. The AISI 4340 steel is chosen because it has typical

tempered martensite, and its relationship with crack growth can be better characterized by SEM. The main objective is to fully understand the fatigue crack branching, deflection and growth mode. The detailed microscopic analysis of the fracture surface reveals the different fracture characteristics and the mechanism operating along the crack propagation mode at different stages of crack propagation.

2. Experimental procedures

The AISI 4340 steel by double vacuum smelting was adopted in this study. The elemental compositions are shown in Table 1. The specimens were heated at 850 °C for 1 h then oil quenched and tempered at 204 °C for 2 h, and the torsional yield strength is 932 MPa. The microstructure is typical tempered martensite as shown in Fig. 1, and the EBSD result in Fig. 1b indicates that there are full of BCC phases.

Table 1 Elemental compositions of the experimental AISI 4340 steel (wt.%).

C	Mn	Si	P	S	Cr	Ni	Mo	As	Cu	Fe
0.40	0.80	0.28	0.005	0.0027	0.86	1.95	0.26	0.005	0.02	Bal.

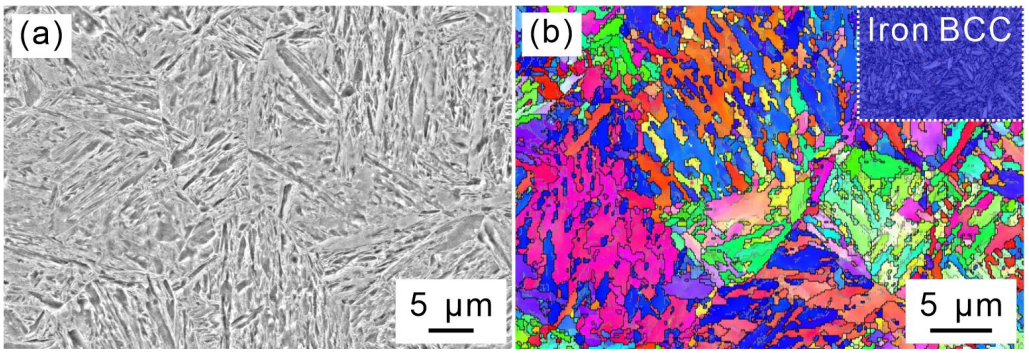

Fig. 1 The microstructures of AISI 4340 steel tempered at 204 °C for 2 h. (a) SEM. (b) EBSD.

The torsional fatigue test, using specimens with a gauge section Φ5.5×30 mm^2, was carried out on the Instron 8874 test machine with a stress ratio of R = -1. The stress amplitudes are every 30 MPa from 610 MPa to 850 MPa and the loading frequency is 15, 15, 15, 15, 14, 11, 6, 3 and 0.5 Hz, respectively. One specimen was tested for each stress level. The tests for fatigue crack growth rate were carried out on the Instron 8801 test machine using the compact tension specimen with size of 10×50×48 mm^3. The loading frequency was 30 Hz and the stress ratio was 0.15.

Electro-etching was used to reveal the microstructures around the fatigue crack. The compositions of the etchant were 10% $HClO_4$ and 90% alcohol. The specimens were etched for 1 min at voltage of 12 V. The fractographies of specimens were observed by the FEI Inspect F50 scanning electron microscope (SEM). The images of the microstructure were taken by the ZEISS sigma 500 SEM.

3. Results

3.1. Fatigue fractographies

In the present study, in total 9 stress amplitudes were adopted in the torsion fatigue test and 8 specimens finally failed. The 8 fracture specimens can be divided in to three types as shown in Fig. 2. When the mode I crack propagation transits to mode II, there would be two optional directions i.e., axial and circumferential due to that both the two directions are in the maximum shear stress plane. The mode II crack propagation would have the maximum driving force in the two directions. Since there are two mode II

crack in each fracture, there would be in total three possible combinations of the mode II crack propagation and all three of them occur in the present study.

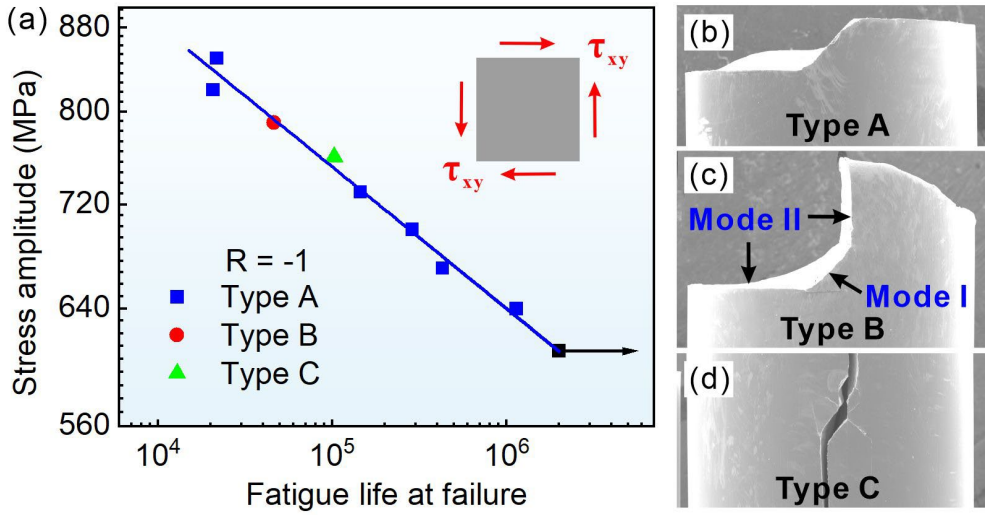

Fig. 2 Three types of torsional fatigue fractures. (a) The relationship between the shear stress amplitude and the fracture type. (b) Type A, (c) Type B. (d) Type C.

For the type A fracture, the main crack is S-shaped in the side view. Besides, both two mode II cracks are perpendicular to the axis. The fracture specimens at the shear stress amplitude of 640 MPa and 850 MPa are displayed in Fig. 3a and 3b, respectively. At different stress amplitudes, the fracture morphologies have similar regions. In detail, there is a final fracture area opposite to the initiation site. As the shear stress amplitude increases, the mode I region becomes smaller, and the final fracture region becomes bigger. At high stress amplitude, a typical factory-roof morphology could be seen as shown in Fig. 3b. The factory-roof morphology in the torsion fatigue fracture of cylindrical specimen is formed by mode I crack branching from mode III cracks [25].

For the type B fracture, one mode II crack is perpendicular to the axis while the other is along the axial direction. Only one fracture (at 760 MPa) occurred in this type

as shown in Fig. 2c and 3c. It is the crack growth perpendicular to the axis that finally leads to the failure of the specimen.

For the type C fracture, both two mode II cracks are along the axial direction. Also, only one fracture (at 790 MPa) belongs to this type as displayed in Fig. 2d and 3d. Although there are two cracks along the axial direction, the final fracture is due to the propagation of circumferential cracks, which are secondary cracks initiated on the main crack, as revealed in Fig. 3d.

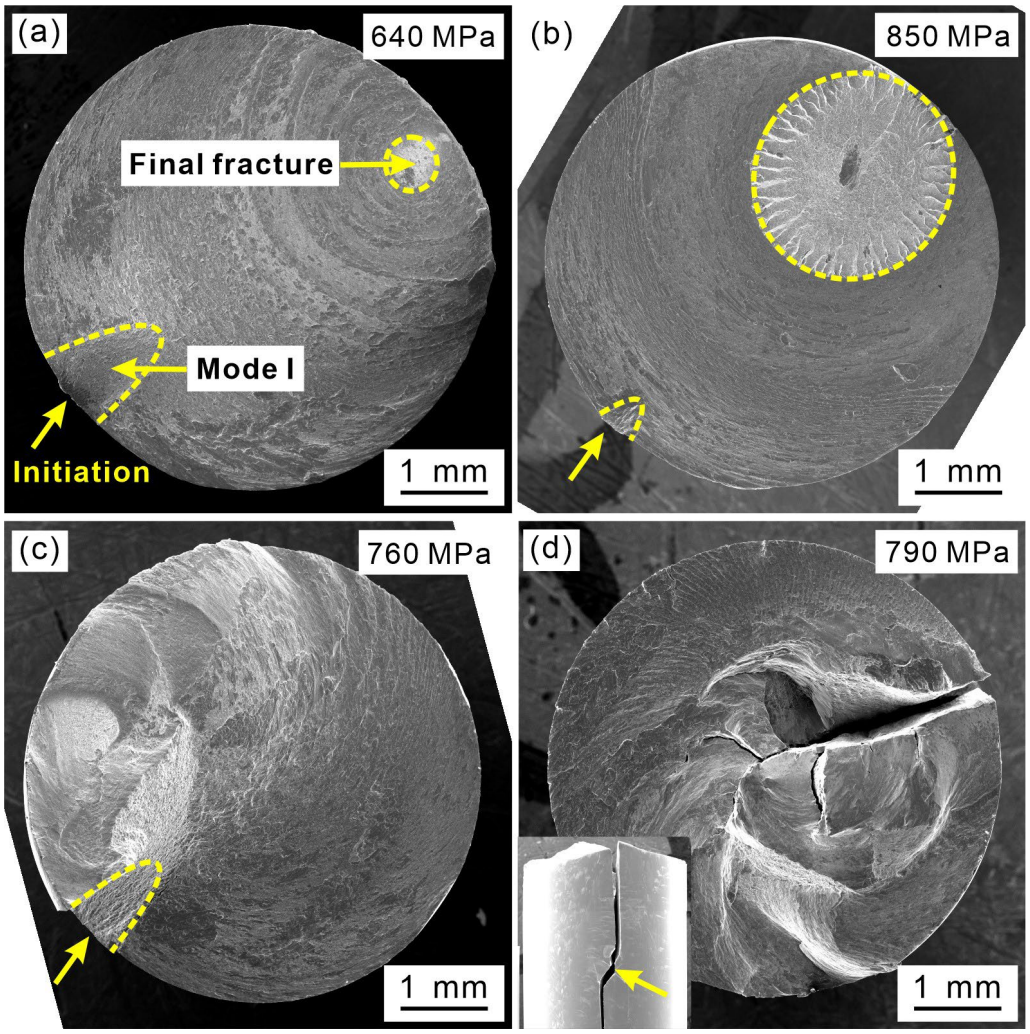

Fig. 3 Three types of torsional fatigue fractures. (a) and (b) Type A. (c) Type B. (d) Type C fracture.

The fatigue fracture can be divided into three regions: fatigue crack initiation region, mode I crack growth region, mode II crack growth region, mixed mode crack growth region and final fracture region. The corresponding features of the type I fracture were observed in detail. Fig. 4 displays the images of initiation site and mode I crack growth region of the torsional fatigue specimen. Fig. 4a and 4b shows the high magnification image of the initiation site from the side and top view, respectively, and a smooth platform could be seen. The platform is along the maximum shear stress plane. After propagating a distance in mode II, the crack branches into mode I cracks. Fig. 4c and 4d show the mode I crack from the side and top view, respectively. The obvious contrast difference in Fig. 4d shows the semi-elliptical edge of the mode I crack.

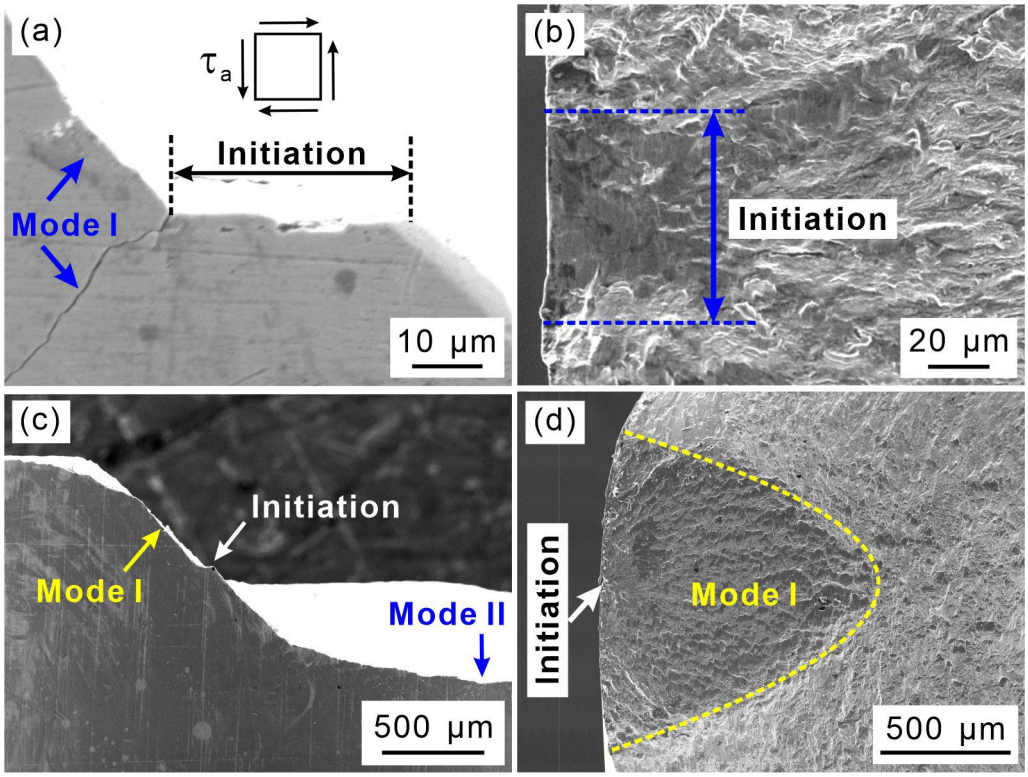

Fig. 4 The SEM images of (a and b) initiation and (c and d) mode I crack of specimen at stress amplitude of 640 MPa.

Fig. 5 shows the fracture morphologies of mode II crack growth region, the mixed mode crack growth region and the final fracture region of the torsional fatigue specimen. The characteristic locations are marked in Fig. 5a, and the high magnification images are displayed in Fig. 5b-f. For the mode II crack growth region, it could be clearly seen that there are fatigue striations near the specimen surface, which indicates the crack propagation direction, as shown in Fig. 5b-d. For the mixed mode crack growth region, the scratches on the fracture next to the mode I crack growth region are observed, as exhibited in Fig. 5e. The scratches are usually caused by the contact of two crack faces resulting from the later mode III or mixed mode crack propagation. In addition, the fatigue striation with different pattern and wider spacing are observed, as revealed in Fig. 5f. The widths of the striation spacing in Fig. 5d and 5f are about 5 μm and 10 μm, respectively. The wider spacing of the striation generally means a later cracking in time.

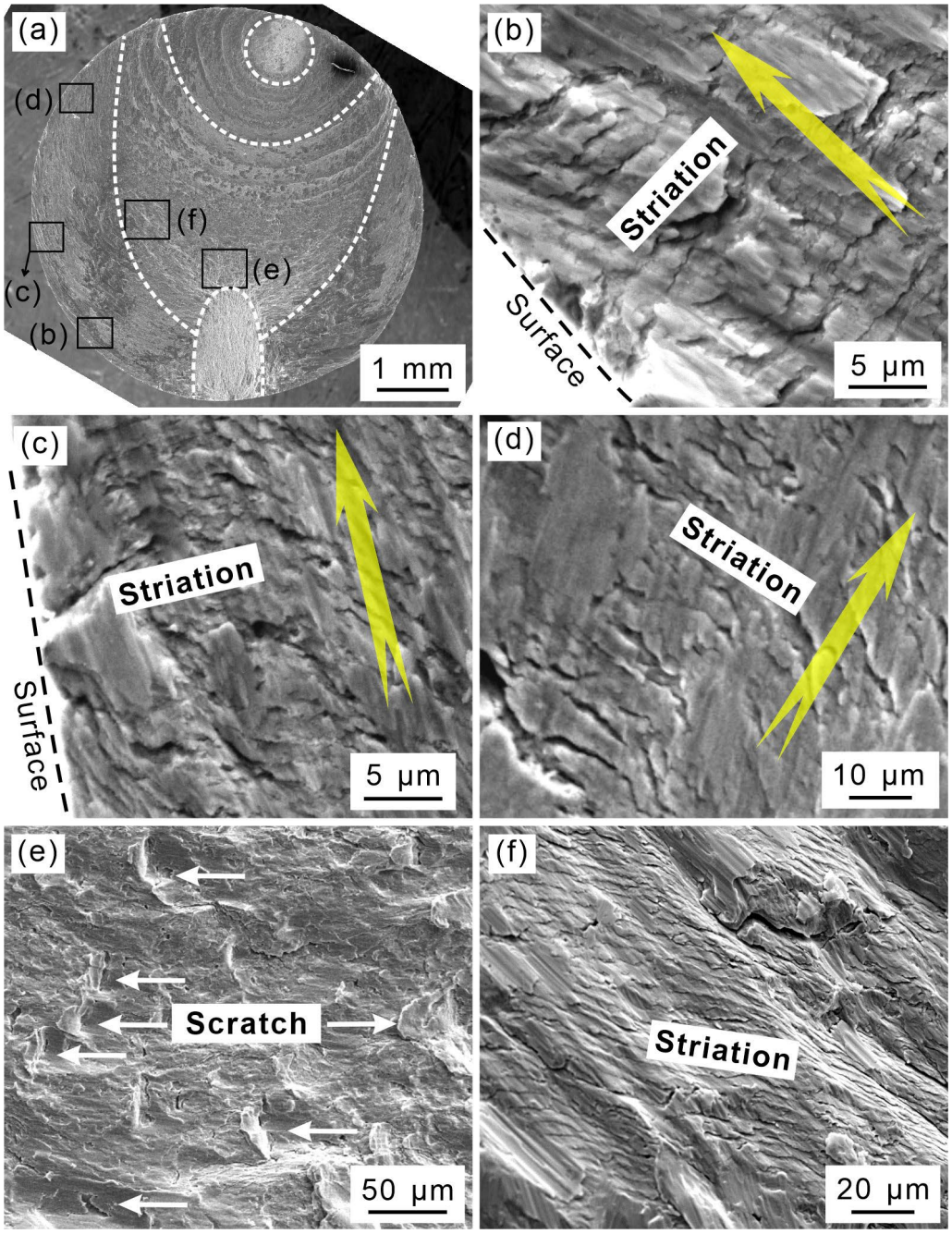

Fig. 5 The SEM images of the fracture morphology of stage II cracks of the torsional fatigue specimens at shear stress amplitude of 640 MPa.

To make a summary, Fig. 6 schematically illustrates the fracture characteristics of the torsional fatigued specimen. The fatigue striations near the specimen surface are in mode II and the fatigue striations inside the specimen are in mixed mode. Based on the fracture characteristics, the sequence of fatigue crack growth can be summarized. The

crack first initiated on the specimen surface and then propagated in mode I to form a semi-ellipse region. Subsequently, the crack propagated circumferentially in mode II along the specimen surface. With the crack propagation, the remaining cross-sectional area became smaller and smaller. When the critical value is reached, the internal crack in mixed mode begins to propagate and gradually turns to unstable crack until the final fracture.

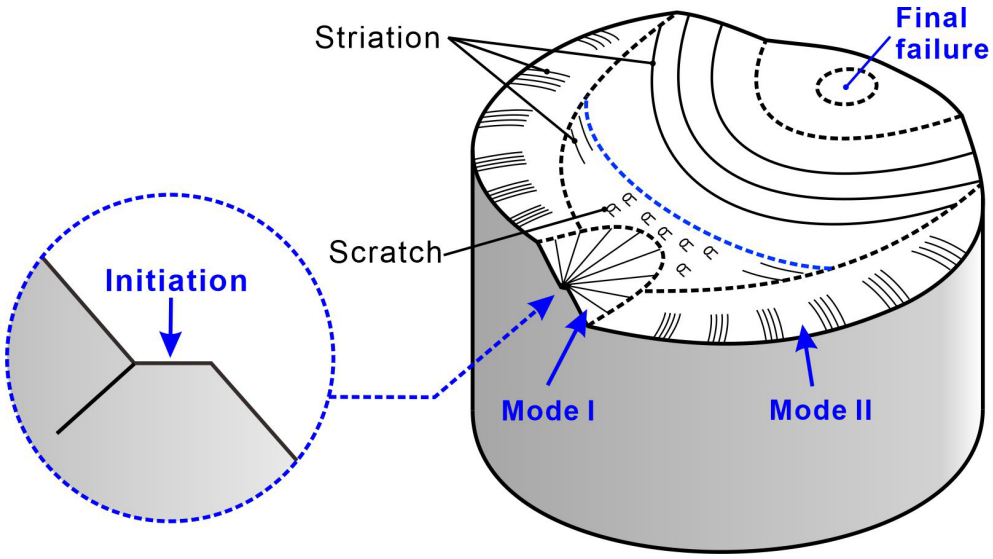

Fig. 6 The schematic illustration of the fracture of the torsional fatigue specimen. The striations near the specimen surface are consecutive.

3.2. Crack length of different mode

The different regions occurred on the fracture surface are attributed to the crack mode transition during the crack growth. Therefore, the crack lengths of different regions were measured from the side view. As shown in Fig. 4a, the crack before branching, as well as mode changing, is defined as the initiation crack. The relationship between the shear stress amplitude and the initiation crack length is plotted in Fig. 7. As the shear stress amplitude increases, the initiation crack length decreases.

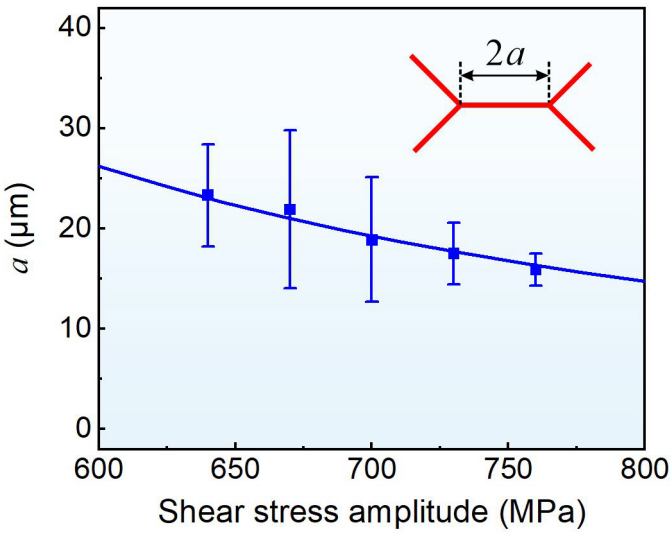

Fig. 7 The relationship between the shear stress amplitude and the initiation crack length.

The subsequent crack growth paths including mode I crack, mode II crack and the transition between them are displayed in Fig. 4c. The fracture is centrosymmetric, and the center of symmetry is the initiation site. The definition of the crack length of mode I and mode II are schematically illustrated in Fig. 8a. Specifically, the mode I crack length is refer to the longest pure mode I crack, and the mode II crack length refer to the shortest pure mode II crack. These two definitions annotate the beginning and end of the crack mode changing. The statistical crack length results of different mode for specimen under different shear stress amplitude are shown in Fig. 8b. As the shear stress amplitude increases, the crack length of both mode I and mode II decreases.

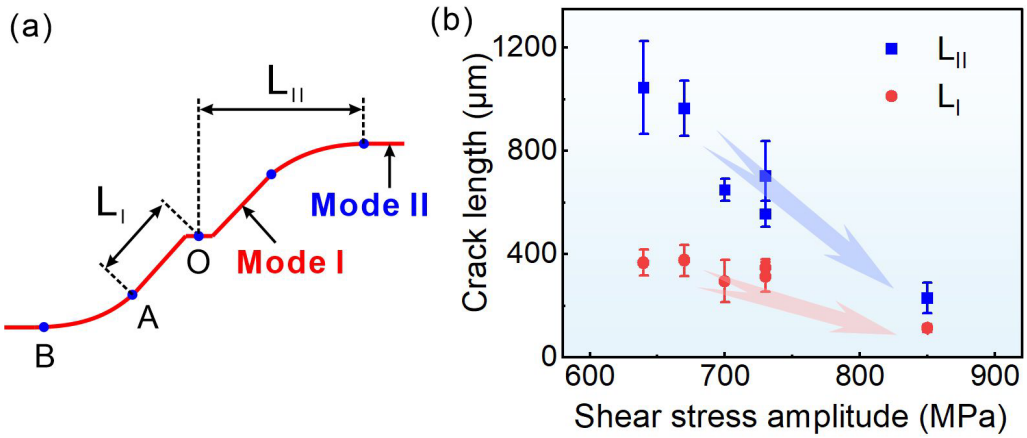

Fig. 8 The observation of the fracture from the side view. (a) Schematic illustration of the definition of crack length. (b) The statistical results of different crack mode for specimen under different shear stress amplitude.

3.3. Relation between fatigue crack and martensitic lath

For the specimen at shear stress amplitude of 760 MPa, more cracks could be observed apart from the main crack as shown in Fig. 9. Each initiation crack has 4 branches in mode I. There are two pairs of branches perpendicular to each other on each side of the initiation crack. On the other hand, branches in the same direction could be grouped. Therefore, there would be a pair of short branches and a pair of long branches as shown in Fig. 9a and 9b. In the meantime, there would also be the cases that all four branches have the same length as shown in Fig. 9c and 9d.

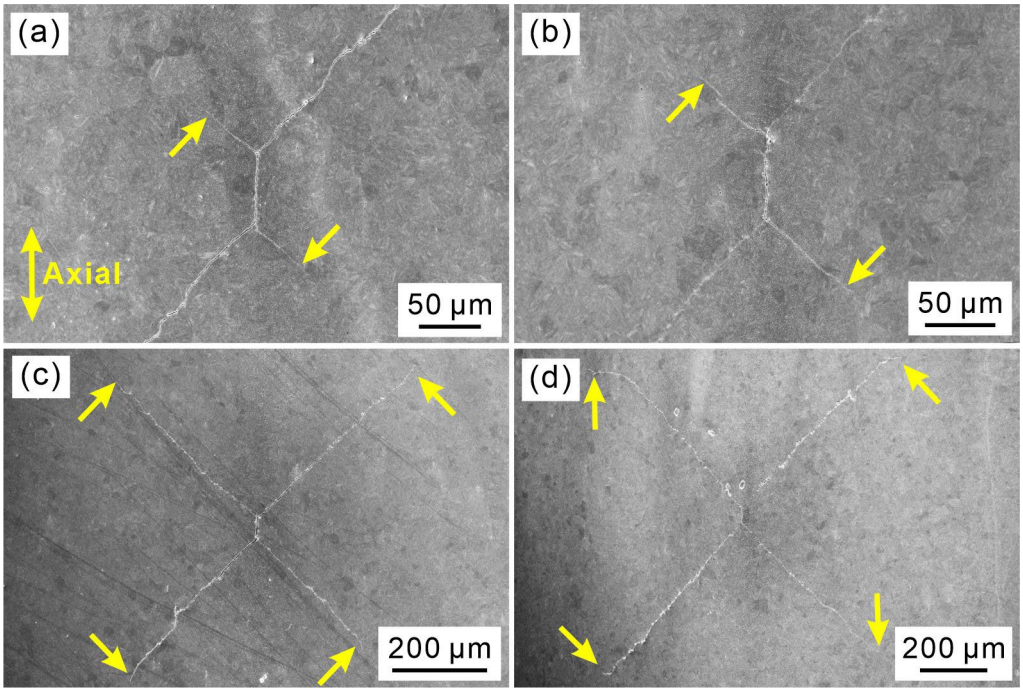

Fig. 9 Two pairs of branches with different length on specimen at stress amplitude of 760 MPa. The crack tips are marked by the arrows.

The microstructures around the branch were examined carefully, and the images are displayed in Fig. 10 and 11. The characteristics of the crack growth path correlated with the microstructure in Fig. 10a are enlarged as shown in Fig. 10b-d. Firstly, the crack propagates along the lath, and the angle between the lath and the axial direction is about 45° as shown in Fig. 10b. Secondly, the crack growth path has a large deflection when encountering the boundary, as shown in Fig. 10c. Thirdly, the crack growth path would be zig-zag, when the crack passes through a lath packet whose direction deviates greatly from 45°. This was also observed in a maraging steel under axial tension-compression fatigue test [26].

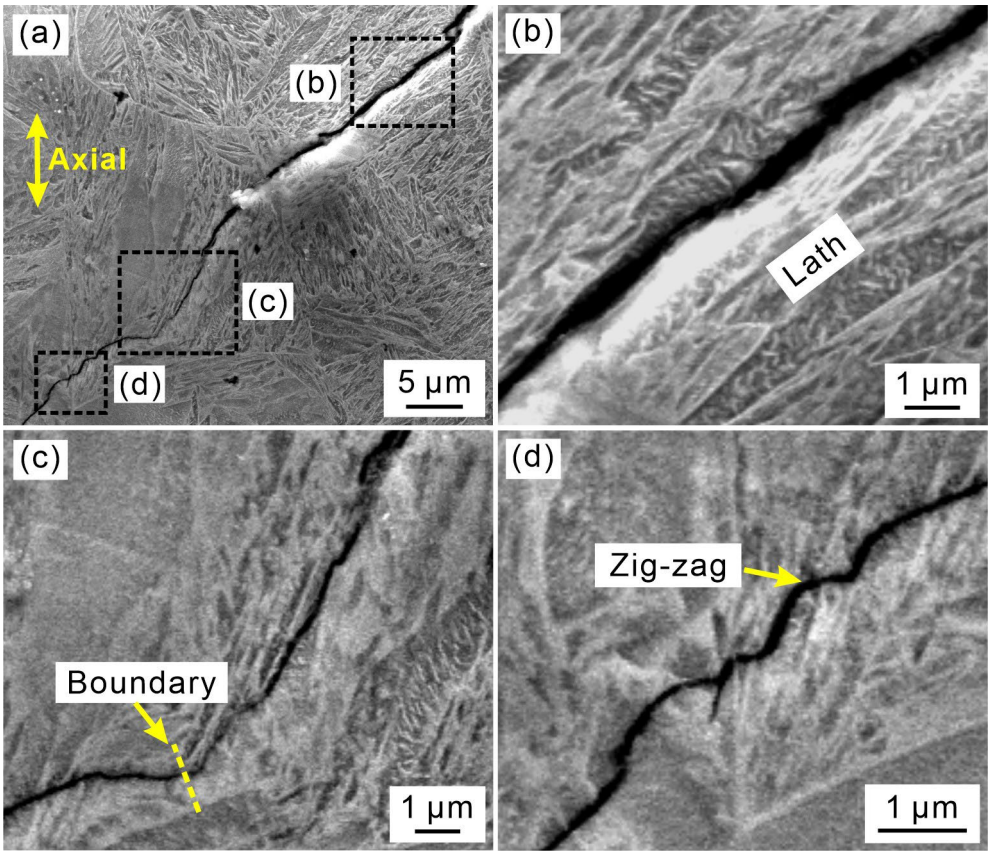

Fig. 10 The microstructure along the crack propagation paths on specimen at stress amplitude of 640 MPa. (a) Overall view. (b) Path along the lath. (c) Deflection around the boundary. (d) Zig-zag path.

Fig. 11 displays the microstructure around the tips of the branches. It is clear that the crack is arrested at the packet boundary. This suggests that the grain or packet boundary is a barrier for the crack propagation. It is reported that the origin of the barrier effect for the boundary to the fatigue crack is the different crystallographic slip systems in the adjacent grains [27, 28]. Nevertheless, the crack does not stop growing, but is arrested for a few cycles. With the continuous loading, the crack would eventually pass through the boundary.

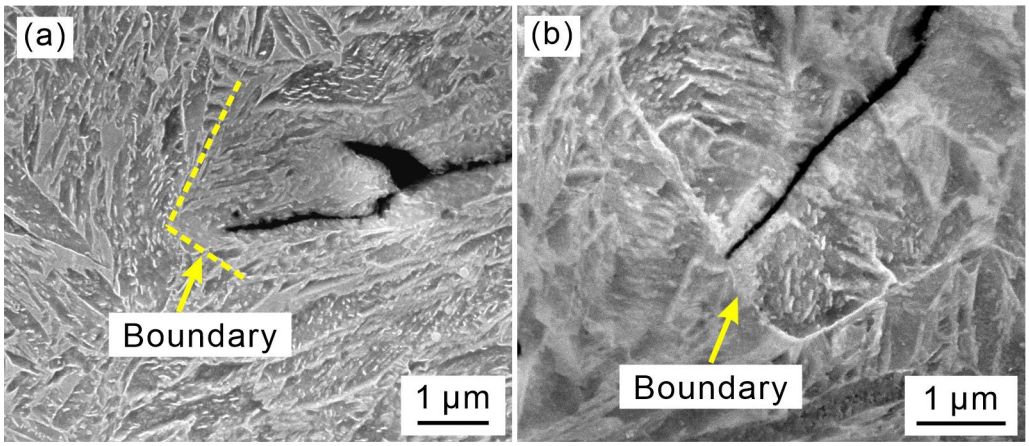

Fig. 11 The microstructures around the arrested crack tips on specimen at stress amplitude of 640 MPa. The original austenite grain boundary or the martensitic packet boundary are marked by arrows.

4. Discussion

Based on the above results, there are several transitions during the fatigue crack initiation and propagation, including 1) initiation crack to mode I branches and 2) mode I crack to mode II crack. Besides, there is competition between the two pairs of branches. The reasons for these transitions and competition will be analyzed.

4.1. Initiation crack to mode I branches

Fig. 7 displays the relationship between the stress amplitude and the initiation crack length. With the increase of the stress amplitude, the initiation crack length decreases gradually. This phenomenon was also reported in a high-strength steel and 316L stainless steel [12]. It is believed that the transition from initiation crack to mode I branches is determined by whether mode I crack begins or not. For the same applied stress, a mode II crack would have a larger plastic zone than a mode I crack [15, 29]. More energy will be absorbed in a mode II crack because of the lager plastic zone.

Furthermore, the transition is determined by whether the fatigue crack stress intensity factor (SIF) reaches $K_{\mathrm{I,th}}$ or not [15]. The SIF is calculated by:

$$K_{\mathrm{I}} = \frac{\tau_{\mathrm{a}}\sqrt{\pi(\cos 45° \, a)}}{\sqrt{1 - \frac{1}{2}\left(\frac{\tau_{\mathrm{a}}}{\tau_{\mathrm{YS}}}\right)^2}}, \tag{1}$$

where τ_{a} is the stress amplitude, a is half of the initiation crack length, $\cos 45° \, a$ is the projection length perpendicular to the principal stress and τ_{YS} is the torsional yield strength. Due to the SIF threshold $K_{\mathrm{I,th}}$ is a material constant, the relationship between the stress amplitude and the initiation crack length could be given by:

$$a = \left(1 - \frac{1}{2}\left(\frac{\tau_{\mathrm{a}}}{\tau_{\mathrm{YS}}}\right)^2\right)\frac{\sqrt{2}}{\pi}\left(\frac{K_{\mathrm{I,th}}}{\tau_{\mathrm{a}}}\right)^2. \tag{2}$$

The fitting result can be seen in Fig. 7. It shows that the SIF threshold $K_{\mathrm{I,th}}$ is 5.35 MPa·$\sqrt{\mathrm{m}}$, which is reasonable for the present steel when stress ratio is close to zero [30-32].

The microstructure around the branching point was observed and displayed in Fig.12a and 12b. There are three main kinds of crack propagation modes: 1) along the packet boundary, 2) along the lath boundary and 3) perpendicular to the lath. The first two can be understood as that the boundary is the weak region as it is in the fatigue crack initiation situation . As for the crack propagation perpendicular to the lath, it is similar to the zig-zag path in Fig. 10d.

It is possible that the SIF exceeds the threshold before the crack tip before the crack tip reaches the packet boundary. However, due to that the lath boundary are the weak region compared to the lath, the crack prefers to continue propagate along the lath boundary in mode II until the crack approaches the packet boundary. Therefore, the branching mechanism includes two aspects: 1) The SIF of the initiation crack reaches the $K_{\mathrm{I,th}}$. 2) The lath packet in front of the crack is in different direction from the maximum shear stress plane. The schematical illustrations of the driving force for the branching are displayed in Fig. 12c and 12d. As the shear stress reversed, the different pairs of branches start to propagate. This mechanism does not exist in the cyclic normal stress. In addition, when the stress ratio is greater than zero, this phenomenon also does not exist under cyclic shear stress.

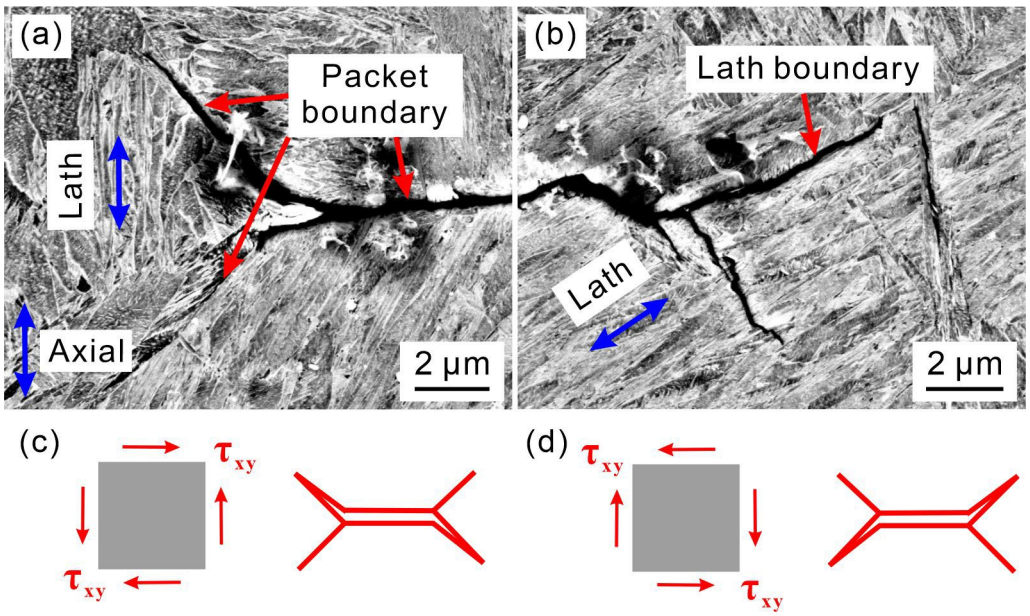

Fig. 12 The branching mechanism. (a) and (b) The images of the microstructures around the branching points. At stress amplitude of 790 MPa. (c) and (d) Schematical illustration of the driving force for the branching.

4.2. Mode I crack to mode II crack

It is believed that the transition from mode I crack to mode II crack is due to the restriction of the hydraulic wedge action grips to the specimen. Schematical illustration of the bending due to the mode I crack is displayed in Fig. 13a. The hydraulic grips could only tolerate limited bending of the specimen. If it was the clamping mode applied in the ultrasonic fatigue machine that one end of the specimen is free, the mode I crack could propagate all the way to the final fracture [33].

Due to the restriction of the grips, although the fatigue crack is growing, the SIF cannot continue to increase, therefore, the fatigue crack is propagating in the form of constant K_I [5]. Unlike the K_I, the K_{II} component continued to increase with the growth of cracks because the mode II crack would not cause the bending of the specimen [5]. Singh et al. [5] studied the changes of K_I and K_{II} component during the transition from mode I to mode II crack in bending-torsional fatigue loading and the limited K_I component is the reason for the transition. In addition, Otsuka et al. [34] found that for 2170-T3 and 7075-T6 alloy, when $K_{II}/K_I > 1.6$, cracks grew in mode II. When K_{II}/K_I was less than 1.6, the crack would grow in mode I [34]. Therefore, the propagation behavior of the fatigue crack can be characterized by dividing the crack path into three parts: pure mode I part, transition part and pure mode II part. The SIF of mode I at the end of the transition equals to the value at the start of the transition due to the constant K_I propagation caused by the hydraulic grips. Therefore, the SIF of mode I and mode II component at the end of the transition region can be calculated, and the results are

shown in Fig. 13b. For the present steel, when $K_{II}/K_I > 1.5$, cracks grew in mode II. Besides, the K_I of all the specimens is below 25 MPa·$\sqrt{m}$, which may be the maximum allowable SIF of mode I crack under the hydraulic grips.

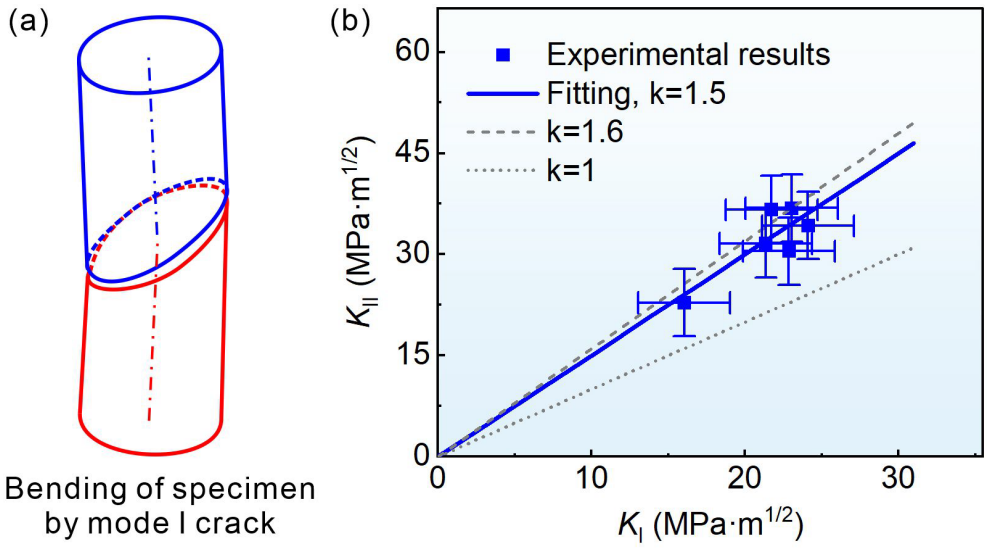

Fig. 13 Mechanism of crack mode change from mode I to mode II. (a) Schematically illustration of the bending deflection due to the mode I crack. (b) The relationship between the stress intensity factors of mode I crack and mode II crack.

4.3. The competition of two branches

As shown in Fig. 9, during the cyclic torsional loading, the initiation crack would branch off into four cracks. They can be the same length, or a pair of long and a pair of short cracks. In another words, the difference in crack growth rate leads to the above results. The reasons can be discussed from several aspects as following.

Firstly, when the four branches are considered together, the propagation pattern is special. In terms of fracture mechanics, each pair of diagonal cracks is closely related, because the calculation of their SIFs at the crack tips shares the same length value *a*. The crack propagation at one branch would lead to the simultaneous increase of the SIF

at the crack tip at both branches. Similarly, the retardation of the crack propagation at one branch will also cause the propagation of both branches to slow down simultaneously.

Secondly, the reason for retardation of propagation can be discussed in two stages. 1) All four branches are in mode I crack growth region; 2) The leading pair of branches enters the mode II crack growth region, while the backward pair of branches are still in mode I crack growth region. In the first stage, the two pairs of cracks are 90° to each other, and the propagation of each pair of cracks does not affect each other. The retardation of the crack propagation at this stage is due to the influence of the microstructure, namely the packet boundary. It is well known that the grain boundary could arrest the short fatigue crack [28, 35-40]. Recently, Ueki et al. [41] found that the lath boundary could enhance the crack propagation resistance due to the activation of out-of-plane slips with their Burgers vectors having no component of the crack growth direction. In order to study the influence of boundary on crack growth, the suspension of different cycles from 1000 to 4000 was manually imposed. The different cycles reflect the suspension of different numbers of encountered boundaries. The fatigue crack growth rate adopted is as:

$$da/dN = 2.88 \times 10^{-8}(\Delta K)^{2.60}. \quad (3)$$

As shown in Fig. 14a, the crack lengths are 70%, 49%, 37% and 28% for delay of 1000, 2000, 3000 and 4000 cycles, respectively, compared to the crack length with no

delay. The total propagation cycles are 30000 and the delay of 2000 cycles could reduce the final crack length by half. Therefore, although the lath packets are randomly distributed, if the number of boundaries encountered by each pair of cracks is slightly different, this blocking effect will be obviously reflected in the final crack length.

In the second stage, when the leading pair of branches enters mode II crack growth region, the two pairs of cracks are not 90° to each other anymore, as shown in Fig. 14b. Because of stress redistribution in mode I component, the driving force of the backward pair of branches will be further reduced, and the growth rate will be further diminished.

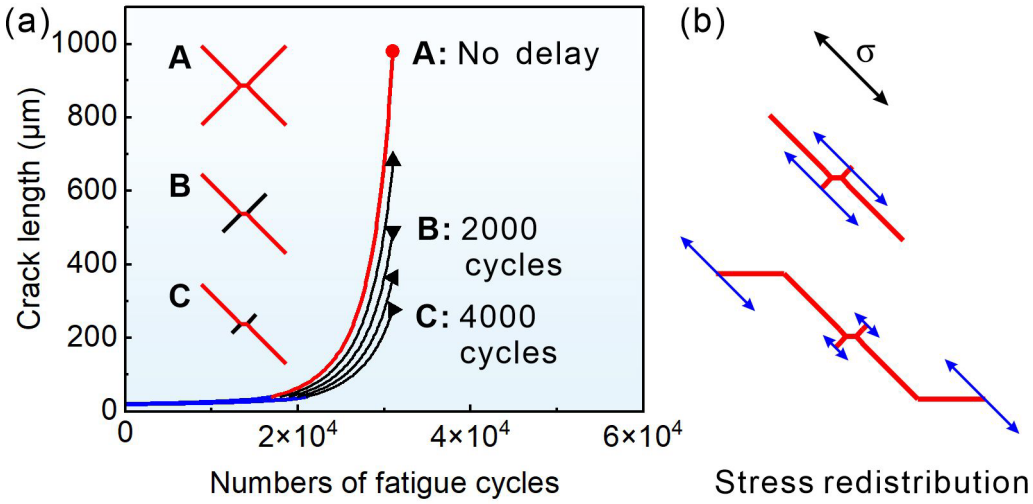

Fig. 14 The mechanism for the retardation in two stages of the fatigue crack propagation (a) The relationship between the crack length and the cycles of delay in the first stage. (b) Stress redistribution caused by the growth of the leading crack branches in the second stage.

5. Conclusions

The high-cycle torsional fatigue crack propagation behaviors of AISI 4340 steel were studied in this work. Based on the experimental results and discussions, the main conclusions for high-cycle fatigue regime are summarized as follows:

1) When $K_{\mathrm{I}} > K_{\mathrm{I,th}}$ and the crack tip reaches the packet boundary different from the maximum shear stress plane, the initiated crack would branch off to four cracks in mode I. There are three main kinds of crack propagation mode when branching: along the packet boundary, along the lath boundary and perpendicular to the lath.

2) Due to the restriction of the grips, when the crack encounters the transition region, the crack propagates in constant K_{I} mode. The K_{II} component continued to increase with the growth of cracks. When $K_{\mathrm{II}}/K_{\mathrm{I}} > 1.5$, the crack grows in mode II.

3) There is a competitive relationship between different pairs of branches. The backward pair of branches fall behind due to that they encountered more boundary barriers and theirs driving force were reduced by the stress redistribution caused by the leading pair of branches.

Data availability

Data will be made available on request.

Credit authorship contribution statement

Z.K. Xu: Conceptualization, Formal analysis, Investigation, Data curation, Writing - original draft. **B. Wang:** Resources, Writing – review & editing. **P. Zhang:** Conceptualization, Methodology, Supervision, Writing - review & editing. **Z.F. Zhang:** Supervision, Writing - review & editing.

Acknowledgments

This work was financially supported by the National Science and Technology Major Project of China under grant No. J2019-VI-0019-0134, the Strategic Priority Research Program of the Chinese Academy of Sciences under grant No. XDC04040502, National Natural Science Foundation of China (NSFC) under grant Nos. 52130002 and 52001310, IMR Innovation Fund under grant No. 2022-PY06, the Special Fund Project of High-tech Industrialization Cooperation between Jilin Province and CAS under grant Nos. 2020SYHZ0008 and 2021SYHZ0046, the Open Research Fund from the State Key Laboratory of Rolling and Automation, Northeastern University under grant No. 2021RALKFKT004.

References

[1] J.Z. Chen, B. Zhang, Z.M. Song, H.Y. Wan, G.P. Zhang, Influence of pre-torsion angles on torsion fatigue properties of 45CrMoVA steel bars, Int. J. Fatigue 137 (2020) 105645.

[2] S. Mobasher Moghaddam, J.A.R. Bomidi, F. Sadeghi, N. Weinzapfel, A. Liebel, Effects of compressive stresses on torsional fatigue, Tribol. Int. 77 (2014) 196-210.

[3] N. Gates, A. Fatemi, Friction and roughness induced closure effects on shear-mode crack growth and branching mechanisms, Int. J. Fatigue 92 (2016) 442-458.

[4] X.w. Wang, S.j. Dong, C.l. Zhang, B. Jiang, Analysis of torsion bar failure occurring during the pre-strained manufacturing for heavy off-road tracked vehicles, Eng. Fail. Anal. 133 (2022).

[5] A.K. Singh, S. Datta, A. Chattopadhyay, J.C. Riddick, A.J. Hall, Fatigue crack initiation and propagation behavior in Al – 7075 alloy under in-phase bending-torsion loading, Int. J. Fatigue 126 (2019) 346-356.

[6] B.M. Schönbauer, K. Yanase, M. Chehrehrazi, M. Endo, H. Mayer, Effect of microstructure and cycling frequency on the torsional fatigue properties of 17-4PH stainless steel, Mater. Sci. Eng. A 801 (2021) 140481.

[7] L. Pallarés-Santasmartas, J. Albizuri, A. Avilés, N. Saintier, J. Merzeau, Influence of mean shear stress on the torsional fatigue behaviour of 34CrNiMo6 steel, Int. J. Fatigue 113 (2018) 54-68.

[8] B.M. Schönbauer, K. Yanase, M. Endo, Influences of small defects on torsional fatigue limit of 17-4PH stainless steel, Int. J. Fatigue 100 (2017) 540-548.

[9] A. Fatemi, R. Molaei, S. Sharifimehr, N. Shamsaei, N. Phan, Torsional fatigue behavior of wrought and additive manufactured Ti-6Al-4V by powder bed fusion including surface finish effect, Int. J. Fatigue 99 (2017) 187-201.

[10] S. Beretta, S. Foletti, K. Valiullin, Fatigue strength for small shallow defects/cracks in torsion, Int. J. Fatigue 33(3) (2011) 287-299.

[11] Y. Akiniwa, S. Stanzl-Tschegg, H. Mayer, M. Wakita, K. Tanaka, Fatigue strength of spring steel under axial and torsional loading in the very high cycle regime, Int. J. Fatigue 30(12) (2008) 2057-2063.

[12] W. Zhang, R. Akid, Mechanisms and fatigue performance of two steels in cyclic torsion with axial static tension/compression, Fatigue Fract. Eng. Mater. Struct. 20(4) (1997) 547-557.

[13] K. Tanaka, H. Takahash, Y. Akiniwa, Fatigue crack propagation from a hole in tubular specimens under axial and torsional loading, Int. J. Fatigue 28(4) (2006) 324-334.

[14] A. Nikitin, C. Bathias, T. Palin-Luc, A new piezoelectric fatigue testing machine in pure torsion for ultrasonic gigacycle fatigue tests: application to forged and extruded titanium alloys, Fatigue Fract. Eng. Mater. Struct. 38(11) (2015) 1294-1304.

[15] Y. Murakami, K. Takahashi, Torsional fatigue of a medium carbon steel containing an initial small surface crack introduced by tension–compression fatigue: Crack

branching, non-propagation and fatigue limit, Fatigue Fract. Eng. Mater. Struct. 21(12) (1998) 1473-1484.

[16] U. Karr, B. Schönbauer, M. Fitzka, E. Tamura, Y. Sandaiji, S. Murakami, H. Mayer, Inclusion initiated fracture under cyclic torsion very high cycle fatigue at different load ratios, Int. J. Fatigue 122 (2019) 199-207.

[17] G. Marquis, D. Socie, Long-life torsion fatigue with normal mean stresses, Fatigue Fract. Eng. Mater. Struct. 23(4) (2000) 293-300.

[18] I. Serrano-Munoz, D. Shiozawa, S. Dancette, C. Verdu, J.Y. Buffiere, Torsional fatigue mechanisms of an A357-T6 cast aluminium alloy, Acta Mater. 201 (2020) 435-447.

[19] J.X. Xu, R.H. Li, P. Zhang, Z.F. Zhang, Crack propagation behavior and mechanism of coarse-grained copper in cyclic torsion with axial static tension, Int. J. Fatigue 131 (2020) 105304.

[20] R.H. Li, P. Zhang, Z.F. Zhang, Fatigue cracking and fracture behaviors of coarse-grained copper under cyclic tension–compression and torsion loadings, Mater. Sci. Eng. A 574 (2013) 113-122.

[21] R.H. Li, P. Zhang, Z.F. Zhang, Torsional fatigue cracking and fracture behaviors of cold-drawn copper: Effects of microstructure and axial stress, Acta Metall. Sinica 32(12) (2019) 1521-1529.

[22] R.H. Li, Z.J. Zhang, P. Zhang, Z.F. Zhang, Improved fatigue properties of ultrafine-grained copper under cyclic torsion loading, Acta Mater. 61(15) (2013) 5857-5868.

[23] U. Hofmann, J. Riedle, I. Altenberger, A. Cote, M. Burwell, Ultra-low cycle torsion fatigue of annealed copper, Fatigue Fract. Eng. Mater. Struct. 38(12) (2015) 1432-1442.

[24] A. Fatemi, N. Gates, D.F. Socie, N. Phan, Fatigue crack growth behaviour of tubular aluminium specimens with a circular hole under axial and torsion loadings, Eng. Fract. Mech. 123 (2014) 137-147.

[25] Y. Murakami, K. Takahashi, R. Kusumoto, Threshold and growth mechanism of fatigue cracks under mode II and III loadings, Fatigue Fract. Eng. Mater. Struct. 26(6) (2003) 523-531.

[26] Z.K. Xu, B. Wang, P. Zhang, Z.F. Zhang, Short fatigue crack growth behavior in 18Ni marageing steel, Mater. Sci. Eng. A 807 (2021) 140844.

[27] M. Herbig, A. King, P. Reischig, H. Proudhon, E.M. Lauridsen, J. Marrow, J.-Y. Buffière, W. Ludwig, 3-D growth of a short fatigue crack within a polycrystalline microstructure studied using combined diffraction and phase-contrast X-ray tomography, Acta Mater. 59(2) (2011) 590-601.

[28] F. Briffod, A. Bleuset, T. Shiraiwa, M. Enoki, Effect of crystallographic orientation and geometrical compatibility on fatigue crack initiation and propagation in rolled Ti-6Al-4V alloy, Acta Mater. 177 (2019) 56-67.

[29] D.F. Socie, G.R. Marquis, Multiaxial Fatigue, Society of Automotive Engineers, Warrendale, PA, 2000.

[30] L. Lawson, E.Y. Chen, M. Meshii, Near-threshold fatigue: a review, Int. J. Fatigue 21 (1999) S15-S34.

[31] R.O. Ritchie, Influence of microstructure on near-threshold fatigue-crack propagation in ultra-high strength steel, Met. Sci. 11(8-9) (1977) 368-381.

[32] R.O. Ritchie, Near-threshold fatigue-crack propagation in steels, Int. Met. Rev. 24(1) (1979) 205-230.

[33] A. Nikitin, T. Palin-Luc, A. Shanyavskiy, Fatigue crack initiation and growth on an extruded titanium alloy in gigacycle regime: comparison between tension and torsion loadings, Procedia Struct. Integrity 2 (2016) 1125-1132.

[34] A. Otsuka, K. Tohgo, H. Matsuyama, Fatigue crack initiation and growth under mixed mode loading in aluminum alloys 2017-T3 and 7075-T6, Eng. Fract. Mech. 28(5) (1987) 721-732.

[35] S. Suresh, R.O. Ritchie, Propagation of short fatigue cracks, Int. Met. Rev. 29(6) (1984) 445-76.

[36] W.L. Morris, The effect of intermetallics composition and microstructure on fatigue crack initiation in AI 2219-T851, Metall. Trans. A 9(9) (1978) 1345-1348.

[37] T. Zhai, A.J. Wilkinson, J.W. Martin, A crystallographic mechanism for fatigue crack propagation through grain boundaries, Acta Mater. 48(20) (2000) 4917-4927.

[38] A.W. Bowen, The influence of crystallographic orientation on fatigue crack growth in strongly textured Ti-6A-4V, Acta Metall. 23(11) (1975) 1401-1409.

[39] W.L. Morris, The non-continuum crack tip deformation-behavior of surface microcracks, Metall. Trans. A 11(7) (1980) 1117-1123.

[40] J. Lankford, The growth of small fatigue cracks in 7075–T6 aluminum, Fatigue Fract. Eng. Mater. Struct. 5(3) (1982) 233-248.

[41] S. Ueki, Y. Mine, X. Lu, Y.L. Chiu, P. Bowen, K. Takashima, Effect of geometric lath orientation on fatigue crack propagation via out-of-plane dislocation glide in martensitic steel, Scr. Mater. 203 (2021) 114045.